International Journal of Pharmaceutics 635 (2023) 122725

Contents lists available at ScienceDirect

International Journal of Pharmaceutics

journal homepage: www.elsevier.com/locate/ijpharm

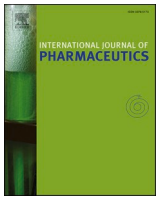

Improvement of drug processability in a connected continuous crystallizer system using formulation additive

Kornélia Tacsi [a,*], György Stoffán [a], Dorián László Galata [a], Éva Pusztai [b], Martin Gyürkés [a], Brigitta Nagy [a], Botond Szilágyi [b], Zsombor Kristóf Nagy [a], György Marosi [a], Hajnalka Pataki [a,*]

[a] Department of Organic Chemistry and Technology, Faculty of Chemical Technology and Biotechnology, Budapest University of Technology and Economics, Műegyetem rkp. 3., H-1111 Budapest, Hungary

[b] Department of Chemical and Environmental Process Engineering, Faculty of Chemical Technology and Biotechnology, Budapest University of Technology and Economics, Műegyetem rkp. 3., H-1111 Budapest, Hungary

ARTICLE INFO

Keywords:
Continuous crystallization
Drug flowability improvement
Crystallization additives
Mixed suspension mixed product removal
Plug flow crystallizer
Acetylsalicylic acid reaction mixture
Design of experiments

ABSTRACT

Continuous crystallization in the presence of polymer additives is a promising method to omit some drug formulation steps by improving the technological and also pharmacological properties of crystalline active ingredients. Accordingly, this study focuses on developing an additive-assisted continuous crystallization process using polyvinylpyrrolidone in a connected ultrasonicated plug flow crystallizer and an overflow mixed suspension mixed product removal (MSMPR) crystallizer system. We aimed to improve the flowability characteristics of small, columnar primary plug flow crystallizer-produced acetylsalicylic acid crystals as a model drug by promoting their agglomeration in MSMPR crystallizer with polyvinylpyrrolidone. The impact of the cooling antisolvent crystallization process parameters (temperature, polymer amount, total flow rate) on product quality and quantity was investigated. Finally, a spatially segmented antisolvent dosing method was also evaluated. The developed technology enabled the manufacture of purified, constant quality products in a short startup period, even with an 85% yield. We found that a higher polymer amount (7.5–14%) could facilitate agglomeration resulting in "good" flowability without altering the favorable dissolution characteristics of the primary particles.

1. Introduction

The crystal habit, size, crystal size distribution (CSD) and polymorphism of the solid crystalline products are crucial regarding the bioavailability or technological properties. Besides purification and separation functions, crystallization became a significant process in the pharmaceutical industry due to its role in designing desired product morphology (Nagy et al., 2020). In addition, continuous crystallization technologies can be operated safer and more economically with a reduced footprint. Thus, the continuous implementation of well-established morphology-modifying batch crystallization methods is an essential field of research.

The most widespread continuous crystallization methods are single- and multi-stage mixed suspension mixed product removal (MSMPR) crystallizers (Yang and Nagy, 2015; Nagy et al., 2020) and tubular crystallizers, such as plug flow crystallizer (PFC), continuous oscillatory baffled crystallizer (COBC), and other types of tubular crystallizers (Mathew Thomas et al., 2022; Mou and Jiang, 2020; Sonnenschein and Wohlgemuth, 2022; Furuta et al., 2016). These are widely applied alone for continuous purification and separation, and only a few publications discuss the combination of different continuous crystallizer equipment that could utilize their advantages. Hu and co-workers used a plug flow reactor (PFR) and a 5-stage continuous stirred tank reactor (CSTR) cascade system for reactive crystallization (Hu et al., 2020). They found that the reaction yield and the final particle size were increased by applying PFR in the first stage due to the supersaturation-reducing effect of the first located PFR. Similar examples where dedicated crystallizer equipment promoting nucleation is connected to an MSMPR crystallizer could be Couette–Taylor equipment (Koyama et al., 2020) or impinging jet crystallizer (IJC) (Tacsi et al., 2021). Liu et al. performed a reactive crystallization connected an IJC (function: feed introduction and reaction) with an MSMPR (function: reaction) and a tubular crystallizer (function: crystal growth) (Liu et al., 2015; Liu et al., 2017). Applying IJC homogeneous nucleation could be initiated, resulting in a narrower CSD product, while the application of a tubular crystallizer could promote higher productivity. The continuous systems connected in the

* Corresponding authors.
E-mail addresses: kornelia.tacsi@edu.bme.hu (K. Tacsi), pataki.hajnalka@vbk.bme.hu (H. Pataki).

https://doi.org/10.1016/j.ijpharm.2023.122725
Received 21 October 2022; Received in revised form 17 January 2023; Accepted 11 February 2023
Available online 17 February 2023

opposite order are more common, thus the combination of first located MSMPR crystallizer with a second located coiled tubular crystallizer (Gao et al., 2018) or COBC (Wu et al., 2021) could be effective to modify product properties. In these systems, MSMPR performs as a continuous seed generator eliminating the risk of blockage and encrustation occurring in the following tubular crystallizer and can provide polymorphic form control. In any arrangement the connected continuous crystallization systems have been mainly used in reactive crystallization. It can be useful to control the supersaturation thus modify the physical properties of the crystals (narrow particle size distribution) and avoiding clogging in a productive continuous process.

Another alternative to modify the physical properties of crystals is additive-assisted heterogeneous crystallization when foreign substrates or additives are applied to influence the crystallization mechanisms by forming mainly secondary or ionic interactions with the drug molecules (Sangwal, 2007). The range of crystallization additives is broad, including tailor-made additives, polymer excipients (Simone et al., 2016), surfactants (Yilmaz et al., 2017), small molecular mass organic and inorganic components, etc. The additives could affect the crystallization process and the product quality in various ways, such as (i) modifying induction time (Pfund et al., 2015; van der Leeden et al., 1993), thus (ii) increasing solubility or bioavailability (Yilmaz et al., 2017); (iii) promoting selective crystallization of polymorphs or cocrystals (Wang et al., 2020), (iv) improve technological properties of crystalline material (Nokhodchi et al., 2010; Kaialy et al., 2014) (v) decrease the possibility of fouling (Acevedo et al., 2019). The drug formulation excipients, mainly polymers, can decrease or, in the case of heteroepitaxial nucleation, increase the nucleation rate. Besides, they can modify crystal growth based on the interactions between drug molecules and polymer chains or similarities in their crystal lattice structures (Borsos et al., 2016). The main purpose of such additive-assisted crystallization is to promote nucleation, or improve technological and functional properties (improved dissolution (Arribas Bueno et al., 2018; Verma et al., 2018), extended release (Rosenbaum et al., 2018)) of drugs, thus simplifying the technological line (Rosenbaum et al., 2018; Erdemir et al., 2018; Erdemir et al., 2019; Schenck et al., 2020).

Additive-assisted heterogeneous crystallization is typically accomplished in batch mode (Arribas Bueno et al., 2018; Verma et al., 2018; Chadwick et al., 2012; Quon et al., 2013); however, some continuous techniques have also recently been published (Yazdanpanah et al., 2017; Testa et al., 2021; Hu et al., 2019). Powell et al. investigated paracetamol (PCM) continuous cooling crystallization in the presence of hydroxypropyl methylcellulose (HPMC) additives in a single-stage MSMPR crystallizer (Powell et al., 2016). This excipient aided crystal habit modification resulting in mostly tabular crystals, and also alleviated fouling and encrustation, supporting the prolonged continuous operation and the application of fouling-sensitive process analytical technology (PAT) probes. Due to the nucleation-suppressing effect of HPMC, the process yield reduction depended on the applied HPMC concentration. Agnew et al. also crystallized PCM metastable polymorph in batch and two continuous crystallization platforms (COBC and MSMPR) in the presence of a structurally similar additive, metacetamol (Agnew et al., 2017). The applied templating molecule facilitated a larger scale polymorph selective manufacture of PCM form II without appearing additive in the final product. Li et al. (Li et al., 2021) and Kutluay et al. (Kutluay et al., 2020) performed continuous crystallization with additives in a single-stage MSMPR crystallizer monitoring the morphology modification effect of additive quality and quantity with various PAT equipment. Overall, the application of polymer additives in continuous crystallization for improving the morphological characteristics of crystalline drugs is under-represented in the relevant literature (Zhang et al., 2017).

In the present research, our goal is to develop a robust connected crystallizer system (PF-MSMPR), including an ultrasonicated PFC (first stage) and an overflow MSMPR crystallizer (second stage) to implement an additive-assisted continuous drug crystallization. An additional aim is to improve the technological properties of the drug (flowability) and thus eliminate the granulation step from the process line while maintaining fast dissolution. To achieve this, a multicomponent acetylsalicylic acid (ASA) reaction mixture was used, which the authors have previously processed by separate continuous crystallizations (Tacsi et al., 2021; Tacsi et al., 2020; Tacsi et al., 2022). In this case, polyvinylpyrrolidone (PVP) as an additive was used to agglomerate fast-dissolving small-sized primary crystals prepared in the PFC. We investigate the effect of temperature, applied polymer amount, total flow rate (TFR) and spatially segmented antisolvent dosing on product quality and quantity to select the most appropriate process conditions.

2. Experimental materials and methods

2.1. Materials

The composition of the multicomponent ASA reaction mixture with the sources of the materials is shown in Table 1; its composition was the same to the synthesis mixture previously produced by flow synthesis (Balogh et al., 2018). The preparation of this ASA reaction mixture was similar to the method published by the authors earlier (Tacsi et al., 2021; Tacsi et al., 2020; Tacsi et al., 2022). Accordingly, the prepared ASA solution concentration was 91.9 mg ASA/mL solution (0.097 g ASA/g solvent mixture) and 4.84 mg SA/mL solution.

The *n*-heptane (>96.0 %) and dichloromethane (DCM, ≥99.0 %) was purchased from Molar Chemicals. The deionized water was produced at the laboratory. The polyvinylpyrrolidone K12 (PVP-K12), polyvinylpyrrolidone K30 (PVP-K30), and polyvinylpyrrolidone K90 (PVP-K90) were donated by Gedeon Richter Plc. Acetonitrile (ACN, >99.9 %), methanol (MeOH, 99.9 %), and cc hydrochloric acid fuming (HCl, 37 %) were obtained from Merck Life Science.

2.2. Experimental methods

2.2.1. The connected plug flow and mixed suspension mixed product removal crystallizer

The schematic image of the connected crystallizer system, including an ultrasonicated PFC and overflow MSMPR crystallizer, is shown in Fig. 1.

The ASA solution was fed continuously with a PU-980 Jasco HPLC pump. Three Syrris ASIA syringe pumps were applied equipped with 10 mL/min maximum flow rate syringe sets for feeding the antisolvent. The antisolvent to ASA solution volume ratio was set to 4:1 in each experiment. The ASA solution and *n*-heptane antisolvent were mixed in a coaxial mixer that was connected to the ultrasonicated PFC. The exact structure of the coaxial mixer is detailed in a previous publication of the authors (Tacsi et al., 2022). The parameters of the PFC made from poly (tetrafluoroethylene) (PTFE) tubing were the following: length 320 cm, inner diameter: 2 mm, outer diameter: 3 mm. The entire PFC tubing is sonicated by placing it into an ASonic PRO 30 type ultrasonic bath (ultrasonic peak power: 240 W, ultrasonic nominal power: 120 W). The sonication frequency was maintained at 40 kHz. The ultrasonic bath was filled with deionized water and ice to temper the system to the required temperature. The temperature in the ultrasonic batch was measured

Table 1
Purity, V//V Ratio, and Source of the Solid Components and Solvents in the Reaction Mixture.

	Purity	V/V %	Source
ASA	99.0 %	–	Sigma Aldrich
SA	99.0 %	–	
Ethyl acetate (EtOAc)	≥99.5 %	79.5	Merck Millipore
Acetic acid (AcOH)	99–100 %	16.3	
Ethanol (EtOH)	≥99 %	3.8	
Phosphoric acid (H_3PO_4)	85 wt%	0.4	

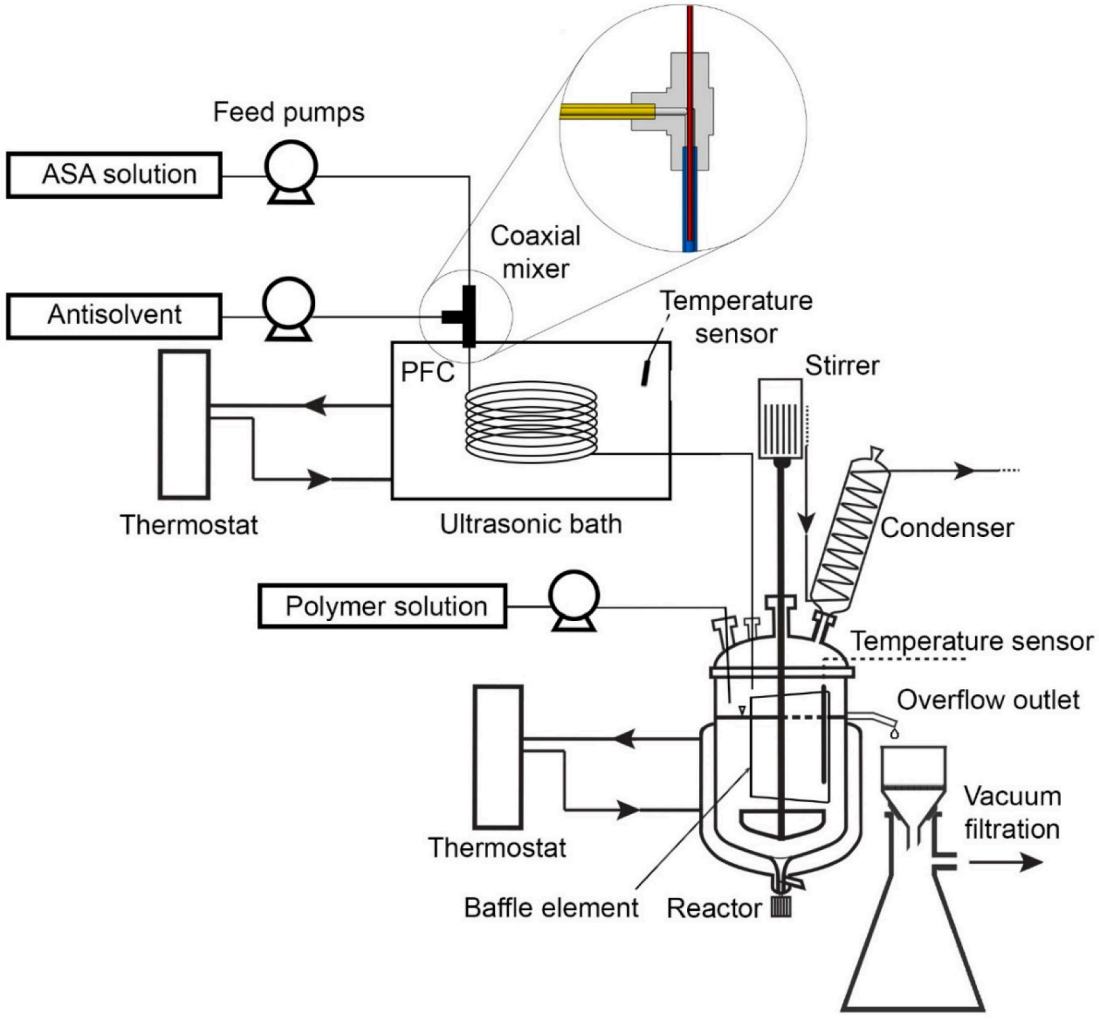

Fig. 1. The schematic image of the connected PF-MSMPR crystallizer system for continuous additive-assisted crystallization.

with a Pt-100 thermometer.

The suspension prepared in the PFC was passed to the MSMPR crystallizer. Simultaneously, the polymer solution was fed continuously into the MSMPR crystallizer with a Pump 33 syringe pump (Harvard Apparatus, USA) equipped with a 10 mL syringe. The MSMPR crystallizer is a 250 mL DN 60 jacketed glass reactor (Schmizo, Schwitzerland) equipped with an overflow tubing (ID: 8 mm), a Eurostar power control-visc type stirrer (IKA, Germany), and a Ruston type 6-blade impeller coated with PTFE (horizontal overall dimensions: 35 mm). The working volume of the reactor was 235 mL. Ministat 230 monofluid thermostat (Huber, Germany) was used for jacket temperature control. The temperature of the slurry was measured with a Pt-100 thermometer. A PTFE vertical plate used as a baffle element was placed into the reactor as described detailed in the previous publication of the authors (Tacsi et al., 2020). The slurry produced in PFC and the polymer solution were fed into the reactor section opposite to the overflow tubing hereby, the crystals must dive under the vertical plate, ensuring uniform residence time distribution of the crystals. The vertical plate was positioned close to and in parallel with the overflow tubing to facilitate homogeneous and representative product removal. The continuous discharge of the suspension from the MSMPR crystallizer was accomplished via the overflow tubing with an equivalent rate to the feeding rate.

The suspension leaving the MSMPR overflow tubing was filtered directly using G4 glass filters connected to a continuously operating diaphragm pump. The crystals were washed with 10 mL *n*-heptane to eliminate the mother liquor remaining on the surface of the crystals. Afterward, the products were dried at room temperature until constant weight, and then the dried ASA samples were weighed (m_s, g). The yield of i^{th} sample ($y_{s,i}$, %) was calculated with the following formulas:

$$m_f = t_f \times \dot{V}_s \times c_s \tag{1}$$

$$y_{s,i} = \frac{m_{s,i}}{m_f} \times 100 \tag{2}$$

where m_f is the nominal fed ASA amount [g]; t_f is the feeding time [min]; $\dot{V}_s$ is the volumetric flow rate of ASA solution [mL/min]; and c_s is ASA solution concentration [g/mL]. The average yield (y_{Av}, %) and its standard deviation (σ, %) was calculated as follows:

$$y_{Av} = \frac{\sum y_{s,i}}{n} \tag{3}$$

$$\sigma = \sqrt{\frac{\sum (y_{s,X} - y_{Av})^2}{(n-1)}} \tag{4}$$

where n [-] is the number of samples.

In the case of the continuous crystallization experimental design and segmented antisolvent dosing experiment, the corrected m_s ($m_{s,i,corr}$) was used to calculate yield. For this, the m_s value was modified with the polymer content determined with Raman spectroscopy (Section 2.2.3.2).

$$m_{s,i,corr} = m_{s,i} \times (1 - \frac{x_{K30}}{100}) \quad (5)$$

At the beginning of the experiment, the following startup strategy was applied. First, we placed 40 mL *n*-heptane into the MSMPR reactor, and this antisolvent was tempered to the desired operating temperature. To make a starting slurry, we pipetted 10 mL of the ASA solution and the polymer solution to heptane into the MSMPR crystallizer during agitation. The volume of polymer solution (600 mg/mL water) added to the starting slurry was determined by the polymer amount (*p*%) we wanted to set for the given experiment (the exact polymer solution volumes are 1 *p*%: 15.3 μL, 7.5 *p*%: 115 μL, and 14 *p*%: 215 μL). Afterward, we started the ASA solution and antisolvent feeding into sonicated PFC. The mixture leaving the PFC was collected separately until the PFC pipe was filled with homogeneous suspension (it lasted for some minutes). This suspension was dripped into starting slurry in the reactor along with the polymer solution.

2.2.2. Continuous experiments in the connected PF-MSMPR crystallizer system

The series of continuous experiments were accomplished based on the Design of Experiments (DoE) principles to investigate the effect of temperature, the total flow rate of ASA solution and antisolvent (TFR) – and thus RT –, and the amount of applied PVP-K30 polymer (*p*%) on the impurity and polymer content of the product, yield, productivity, crystal size, CSD, crystal habit, flowability, and dissolution rate. The set parameter levels of the 2^3 experimental design are summarized in Table 2.

All continuous experiments were performed in the connected PF-MSMPR system. The stirring rate was set constantly at 400 rpm. As the temperature level cannot be set continuously in the ultrasonic bath, this factor was considered a categorical variable. Therefore, the center point measurements were performed separately at the two temperature levels in the center of the continuous variables (*p*%, TFR). The order of the experiments was randomized, and the central point experiments enabled to investigate the repeatability of the results. The TIBCO Statistica (version 13.4) program was used to evaluate the experimental results. The significance level of the statistical analysis was 0.05.

An additional continuous experiment (PF-MSMPR_18) was performed with spatially segmented antisolvent dosing as complementing the DoE. Accordingly, in the PFC, the fed antisolvent amount was equal to the ASA solution volumetric flow rate, while in the MSMPR crystallizer, further antisolvent was added with a 12 mL/min flow rate. The polymer solution (600 mg/mL) was fed into the MSMPR crystallizer with a 0.0460 mL/min feeding rate. The process parameters of this experiment are shown in Table 3.

The continuous experiments lasted 2 to 6 h, which means 15 RTs were investigated in all cases depending on the set TFR. The product leaving the connected crystallizer was sampled 9 times (1, 2, 3, 4, 6, 8, 10, 12, and 15 RTs) at 2 to 5 min intervals depending on the applied feeding rate. The mean RT of the PF-MSMPR system varied depending on set TFR and *p*%, which is shown in the Supplementary Material (Table S1).

2.2.3. Characterization of product quality

2.2.3.1. HPLC analysis. To study the impurity SA content of the product, RP-HPLC analysis was performed according to the HPLC method, which was applied in former publications of the authors (Balogh et al., 2018). The isocratic eluent (40 V/V% water with 0.5 % phosphoric acid and 60 V/V% ACN) flowed with a 1.5 mL/min flow rate in the Supelco Inertsil ODS-2 C18 (GL Sciences, Japan) column. From the wet samples, 1 mg/mL concentration methanol solutions were prepared, and to stabilize the ASA until measurement, it was diluted to 1:20 dilution with a solvent mixture. The determined SA impurity content of the samples was based on the ASA and SA peak areas ratio.

Table 2
Set Crystallization Parameters of the DoE.

	– (lower)	0 (central)	+ (upper)
Temperature [°C]	2	–	25
p% [%]	1.0	7.5	14.0
TFR of ASA solution and antisolvent [mL/min]	10	20	30

2.2.3.2. Raman microspectrometry. We used Raman microspectrometry to study the polymer accumulated on the surface of particles produced by continuous crystallization (called "surface polymer content"). The product was characterized offline with a Labram-type Raman microscopy (Horiba Jobin Yvon, France) equipped with a 532 nm Nd-YAG laser and a CCD detector. For the analysis, 31 × 31-point maps were recorded for one sample at a steady state in each experiment. The Raman measuring conditions were the following: 20x objective, 2 *sec* exposition time, 2x accumulation, 100 μm measuring steps, so 3000 μm × 3000 μm map size.

The spectral concentration of ASA and PVP-K30 was evaluated with the classical least-squares (CLS) method using reference Raman spectra of the pure components. This method is based on the assumption that the sample spectra can be produced as a linear combination of reference spectra. This calculation results in spectral concentrations (x_{ASA}, x_{K30}, %) that is proportional to the mass concentrations of the sample. The resulted polymer spectral concentration data were used to correct the sample mass ($m_{s,i,corr}$, g), that was utilized for yield calculation (eq. (2)).

2.2.3.3. Determination of crystal size, size distribution and habit. The crystal size and CSD plots of each sample were analyzed using an offline Mastersizer 2000 (Malvern Instruments, UK) equipped with a Scirocco 2000 dry powder feeder (Malvern Instruments, UK). We placed appr. 100 mg of the sample into the feeder, which was dispersed with 1 bar overpressure. The measurement lasted for 30 *sec*, followed by a 10 *sec* cleaning section. The final CSD was characterized by volumetric distribution values (D_v10, D_v50, and D_v90). The average D_v-values and its standard deviation of the samples were calculated based on three parallel measurements. The product crystal habit was monitored offline with an Olympus CKX53 inverted microscope equipped with an 18Mp CAM-SC180 Camera set.

2.2.3.4. Flowability analysis. The flowability of the product was measured with an SVM12 type (Erweka, Germany) tapped density tester equipped with 20 mL glass cylinders that were filled with appr. 10 mL sample. The equipment tapped the cylinder 501 times in 167 *sec* until the tapped volume had not changed further. From the measurement, bulk and tapped density were calculated that were used to determine the Hausner ratio ($\frac{\rho_{tapped}}{\rho_{bulk}}$) and Carr index ($\frac{\rho_{tapped} - \rho_{bulk}}{\rho_{tapped}} \times 100$) of the product manufactured in continuous experiments.

2.2.3.5. Dissolution test. In vitro dissolution tests were performed with a Hanson SR8 Plus dissolution tester (Hanson Research, US) equipped with a Hanson Autoplus Maximizer 8 syringe pump sampler (Hanson Research, US). For the measurement, 50 mg of the ASA product was filled into a capsule, and placed into a spiral capsule sinker to prevent the floating of the capsules. The measuring conditions were 900 mL of 0.1 N HCl dissolution medium, 75 rpm stirring rate, and 37.0 ± 0.5 °C medium temperature. During the dissolution test, samples were collected 18 times, every 2.5 min until 20 min, and afterward every 10 min until 120 min. The samples were analyzed with an Agilent 8453 online UV–vis spectrophotometer (Hewlett-Packard, USA) using 5 mL cuvettes. The measurement spectral range was between 190 and 1100 nm. We applied the PLS model built by our research team (Nagy et al., 2021) for the evaluation.

Table 3
Details of Experiment PF-MSMPR_18.

Experiment ID	T [°C]	p% [%]	FR_{ASA} [mL/min]	FR_{AS} [mL/min]	TFR [ml/min]	RT [min]
PF-MSMPR_18	25	7.5	4	PFC: 4 MSMPR: 12	20	12.98

3. Results and discussion

3.1. Preliminary batch and continuous crystallizations

In preliminary batch and continuous experiments, we aimed to study the versions of different molecular weight polyvinylpyrrolidone (PVP-K12, PVP-K30, and PVP-K90) and the effect of baffle element and stirring rate to narrow down the parameters of the investigated experimental space and to select its limit values. These results are discussed in detail in Supplementary Material. According to the batch experiment results, the PVP-K12 additive was not recommended as it does not facilitate agglomeration in smaller amounts, while in higher quantities, a polydisperse product was produced that is difficult to handle. The application of PVP-K30 was beneficial because it promoted the agglomeration of the primer particles while applying 7.5 p% PVP-K30/water (600 mg/mL), and the degree of agglomeration and yield were also high. The PVP-K90 had no morphology modification effect (Table S2). Thus, 600 mg/mL PVP–K30/water feed solution was used in the continuous experiments.

In order to reduce the number of experimental parameters, it was necessary to fix the settings required for representative product removal by preliminary continuous experiments (Table S3-S4). Therefore, the presence of the baffle element and stirring rate was investigated together on process yield and product quality. It can be concluded that without the baffle element (PF-MSMPR_2), the product withdrawal was not representative since the reactor yield was ~ 30 % higher than the average yield of the samples, and the agglomerates were enriched in the reactor. In contrast, the presence of the vertical plate could facilitate the product withdrawal independently of the stirring rate. In addition, a higher stirring rate can support the disintegration or breaking of crystals and agglomerates in the presence of a baffle element (PF-MSMPR_5). Thus, DoE-based continuous experiments were performed with a lower 400 rpm stirring rate and in the presence of a baffle element.

By investigating the continuous preliminary experiment (PF-MSMPR_1) running without polymer additive revealed that the connection of PFC and MSMPR crystallizer does not result in morphology modification alone (Table S4). The product removed from the PF-MSMPR system was identical to the product removed from the PFC (the first stage of the crystallizer system) and contains small and columnar crystals.

3.2. Continuous experiments in connected PF-MSMPR crystallizer system

To test the connected PF-MSMPR crystallizer system and study the process parameter dependence of product quality and quantity, we performed a 2^3 factorial design. According to the results of preliminary experiments (Section 3.1), the following process circumstances were maintained constant within an experiment: stirring rate (400 rpm), vertical plate in a fixed position, fed PVP-K30/water solution (600 mg/mL). In the DoE-based experiments, the effect of temperature, the applied polymer amount (p%), and the TFR of ASA solution and anti-solvent on product composition (impurity and surface polymer content), yield, productivity, crystal habit, size, CSD, and flowability was investigated. Furthermore, the dissolution rate of PFC, MSMPR crystallizer, and connected PF-MSMPR crystallizer system products were compared.

The onset of steady-state was determined based on the product quality (crystal size, CSD). It was found that the steady-state was reached for the first sampling (1 RT) in each experiment. The startup period could not be monitored with the applied sampling frequency and method.

3.2.1. Characterization of product composition and yield

To describe the exact composition of the continuous experiment products, we determined SA impurity content with HPLC and PVP-K30 excipient content with Raman mapping. The results of the analysis are summarized in Table 4.

The SA loading of the product was significantly reduced from the level of 5 % added as the SA impurity content in the entire experimental series was 0.39 ± 0.21 % on average. It can be stated that the change in SA content did not show a clear dependence on the examined process parameters.

The PVP-K30 content of the products is characterized in only one sample (9th sample collected at 15 RT) of each experiment with 961-point Raman maps. The PVP can be identified by its peak at 933 cm^{-1} in the average spectra of the maps (Raman spectra illustrated in Supplementary Material Fig. S3). Via this analysis, we determined the surface polymer content of the samples. With the CLS evaluation, we proved that the spatial distribution of the polymer on the product surface was homogeneous in the cases of 1, 7.5, and 14 p% as well. As illustrated in Table 5, the sum of surface polymer content was increased by applying a higher polymer amount.

It was found that the PVP-K30 content of the product was affected by the fed PVP-K30 amount, while other process parameters did not modify its value significantly. Accordingly, the surface polymer content in the case of 1, 7.5, and 14 % fed polymer was 3.2 ± 0.4 %, 5.7 ± 1.0 %, and 7.0 ± 0.9 %, respectively. In the case of 14 p% experiments, only half of the fed amount appeared in the sample, while in central point experiments (7.5 p%), the ratio of the measured polymer was much higher. It could be assumed that by increasing the fed polymer amount, the PVP-K30 surface content of the product could not increase significantly and presumably reaches a plateau. Otherwise, it is important to note that the PVP is a frequently used formulation additive; thus, its presence in the product cannot be considered an impurity to be removed.

The product crystallinity was proved by comparing the average spectrum from the Raman maps with the spectra of the pure reference components (ASA, SA, PVP) and the DSC and the XRPD of crystalline commercial ASA. These results are presented in the Supplementary Material Fig. S1 Fig. S2 Fig. S3.

As the fed PVP-K30 polymer solution amount was even 14 % compared to the ASA active ingredient thus, the PVP-K30 must be considered during the yield and productivity calculation. The corrected yield (y_{corr}, %) was calculated using eqs (2) and (5). The yield was constant during the whole experiment with a low standard deviation; therefore, the yield (and productivity) of all samples was utilized to calculate the average and standard deviation of the yield and productivity. The corrected yield and productivity values of the experiments are summarized in Table 4 as well. Based on this, the corrected yield was ranged from 63 to 85 %, while the productivity varied from 7.3 to 28.1 g/h. The yield in the PF-MSMPR crystallizer system was similar to that obtained in the previously published separate PFC (Tacsi et al., 2022) and separate MSMPR crystallizer (Tacsi et al., 2020). Thus, it could be assumed that the PVP-K30/water solution did not increase the solubility of the ASA.

3.2.2. Statistical analysis of yield

Statistical analysis was performed to investigate the effect of crystallization process parameters on yield. During continuous experiments in the connected crystallizer system, the level of temperature, polymer amount (p%), and TFR was set considering the rules of DoE. Repeated experiments were performed on center points to investigate the repeatability of the process and to study the linearity of the fitted

Table 4
Result Summary in the Continuous Experimental Series.

ID of exp.	T [°C]	*p*% [%]	TFR [mL/min]	SA [%]	PVP-K30 [%] *	y_{corr} [%] **	Productivity$_{corr}$ [g/h] **
PF-MSMPR_6	2	1	10	0.89 ± 0.11	2.7	80.1 ± 1.9	8.8 ± 0.2
PF-MSMPR_7	2	1	30	0.43 ± 0.09	3.5	79.7 ± 1.8	26.4 ± 0.6
PF-MSMPR_8	2	14	10	0.39 ± 0.04	5.6	78.5 ± 2.8	8.7 ± 0.3
PF-MSMPR_9	2	14	30	0.47 ± 0.08	7.2	85.0 ± 1.4	28.1 ± 0.5
PF-MSMPR_10	25	1	10	0.37 ± 0.03	3.5	66.0 ± 2.9	7.3 ± 0.3
PF-MSMPR_11	25	1	30	0.31 ± 0.15	3.2	63.3 ± 1.5	20.9 ± 0.5
PF-MSMPR_12	25	14	10	0.39 ± 0.17	7.4	69.3 ± 2.1	7.6 ± 0.2
PF-MSMPR_13	25	14	30	0.49 ± 0.19	7.7	66.3 ± 1.3	21.9 ± 0.4
PF-MSMPR_14	2	7.5	20	0.16 ± 0.17	4.7	83.2 ± 1.2	18.3 ± 0.3
PF-MSMPR_15	2	7.5	20	0.33 ± 0.10	5.4	83.5 ± 1.1	18.4 ± 0.2
PF-MSMPR_16	25	7.5	20	0.22 ± 0.14	5.5	65.5 ± 0.8	14.4 ± 0.2
PF-MSMPR_17	25	7.5	20	0.33 ± 0.16	7.0	65.5 ± 0.5	14.5 ± 0.1

* PVP-K30 is a tableting binder, so its presence in the crystalline product cannot be considered a real impurity during the production of an active ingredient.
** Pure ASA yield and productivity corrected with the amount of PVP in the product.

Table 5
Spatial Distribution of PVP-K30 on the Surface of Samples in case of Experiments with 1, 7.5, and 14% Polymer Amount Obtained from Raman Map Evaluation.

PF-MSMPR_7 T:2°C; K30:1*p*%; TFR:30 mL/min	PF-MSMPR_15 T:2°C; K30:7.5*p*%;TFR:20 mL/min	PF-MSMPR_9 T:2°C; K30:14*p*%; TFR:30 mL/min
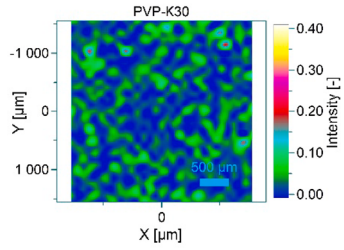	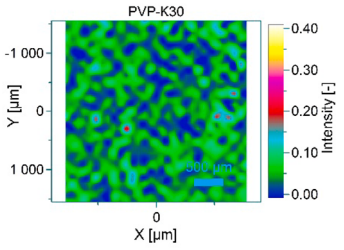	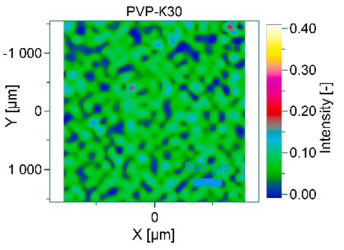

secondary model. The performed 2 by 3 factorial design was orthogonal. The *p*-values, estimated coefficients, and their confidence intervals are summarized in Table 6.

According to prior expectations and the Half normal probability plot (Fig. 2), the temperature significantly affected yield. The curvature, *p*%, and interactions of temperature-TFR and *p*%-TFR were statistically significant (*p*-value < 0.05); however, these effects could be neglected compared to the linear effect of temperature. As the ultrasonication of the PFC initiated the nucleation process, the TFR did not affect yield. Considering these results, the following reduced linear model can be used to describe the yield (y, %), where T represents the temperature [°C].

$$y = 82.69 - 0.68T \quad (6)$$

By studying the diagnostic figures, the model is adequate; as a result, the linear model is considered reliable. To illustrate the temperature dependence of the yield, we generated Response Surface (Fig. 3) with the TIBCO Statistica program.

Table 6
The *p*-values, Estimates, and Confidence Intervals of the Model Coefficients ($R^2 = 0.943$).

Factors	Coeff.	*p*-value	−95 % conf. limit	+95 % conf. limit
Mean	73.46	0.000	72.96	73.95
Curvature	1.00	0.022	0.15	1.86
T [°C] (1)	−7.87	0.000	−8.27	−7.46
p% [%] (2)	1.33	0.000	0.83	1.82
TFR [mL/min] (3)	−0.04	0.864	−0.54	0.45
1 by 2	0.41	0.106	−0.09	0.90
1 by 3	−1.56	0.000	−2.06	−1.07
2 by 3	0.89	0.001	0.40	1.39

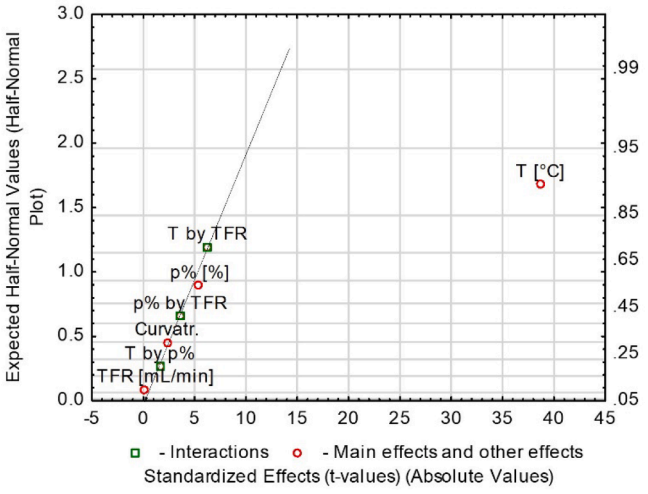

Fig. 2. Half normal probability plot.

3.2.3. *Characterization of crystal Size, Habit, and CSD*

The spatial separation of the crystallization steps (nucleation, crystal growth and agglomeration) has been implemented in the connected crystallizer system. In the PFC, nucleation and crystal growth occurred, and the nucleation was initiated due to intense ultrasonic irradiation. At the same time, the agglomeration process took place in the MSMPR crystallizer, depending on the amount of the added polymer. The amount of the applied polymer additive influenced the crystal size. By adding 1 *p*% PVP-K30 excipient, the ratio of the agglomerates is low, and the product is very similar to the crystals manufactured in a separate PFC regarding crystal habit, size, and CSD. The D_V90 fluctuated 38 ± 5

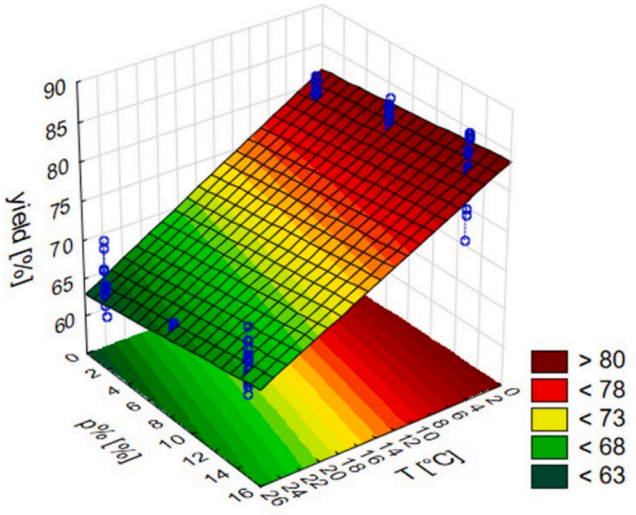

Fig. 3. Response Surface illustrating yield as a function of temperature and *p*% in the experimental region of the performed DoE.

μm on average in the four experiments with 1 *p*% (PF-MSMPR_6,_7,_10, _11). Higher polymer amounts supported the agglomeration of the individual crystals produced in the PFC. Due to the agglomeration, the crystal size increased, the CSD broadened, and the standard deviation of D_v90-values was higher. The average D_v90 was 353 ± 158 μm based on every 14 *p*% experiments (PF-MSMPR_8,_9,_12,_13). The average and standard deviation of D_v-values are illustrated in Fig. 4.

From central point experiments (PF-MSMPR_14-PF-MSMPR_17), it can be concluded that temperature has no significant effect on crystal size, and the variation of D_v90-values is within the limit of standard deviation. In these experiments (1 or 25 °C; 7.5 *p*%; 20 mL/min), the product quality and quantity were similar, the CSD was bimodal, and the standard deviation of D_v90-values was slightly decreased (174 ± 48 μm on average). In the case of 14 *p*% and 30 mL/min TFR, the PVP-K30 excipient could facilitate trimodal CSD of ASA products (Table 7). In contrast, in the case of 14 *p*% and 10 mL/min TFR bimodal CSD was more frequent (Table 8). In these bimodal CSD plots, the sizes of crystal fractions were similar to the experiments with 1 and 7.5 *p*%, but the larger-sized crystal fraction ratio was significantly higher. By applying 14 *p*% and high RT (TFR: 10 mL/min), the degradation of the agglomerates could be supported, resulting in a smaller average crystal size; thus, the TFR could slightly affect the particle size. The effect of *p*% on crystal size, habit, and CSD tendencies is illustrated with the microscopic pictures and CSD plots in Table 7 and Table 8.

A possible mechanism for PVP-induced agglomeration is that the polymer as a binder promotes the bonding of primary plug flow crystallizer-produced crystals through surface interactions (van der Waals, capillary, electrostatic, H-bonding). The coupling of the primary crystals is facilitated by a polymer-rich hydrodynamic boundary layer on the surface of the ASA crystals, in which the polymer is presumably bonded to the crystal by a second-order H-bond. The size and number of agglomerates depend mainly on the amount of polymer applied, resulting in a difference between the products manufactured with 1 *p*% and 7 *p*% polymer amounts.

3.2.4. *Characterization of flowability and dissolution rate*

In each experiment, the flowability of the products was measured to characterize their processability. Flowability categorization was based on the Hausner ratio and Carr index calculated using bulk and tapped density accordingly to Section 2.2.3.4. The average D_v90-values and the classification of each experiment according to the flowability properties are presented in Fig. 5.

The flowability characteristics were primarily influenced by the fed polymer excipient (level of *p*%). By increasing the amount of the polymer solution, the scale of agglomerate formation was higher. The flowability of the agglomerates is better compared to the small and columnar primary crystals. Accordingly, the flowability of the 1 *p*% products was classified as “very poor” or “poor”. In contrast, most of the 14 *p*% experiments were categorized in the “passable” or “fair” category. Thus, the polymer improved the flowability of the crystalline product by several categories in each case.

We also characterized the dissolution profile of a central point PF-MSMPR experiment by comparing the result with two products manufactured in a separate PFC (Tacsi et al., 2022) and a separate MSMPR crystallizer (Tacsi et al., 2020) without polymer. The selected samples were made with similar process settings and reflect the typical products available with the given technology. The presented PFC product contained small, columnar crystals, and its CSD was narrow (D_v10: 3.8 ± 0.3 μm; D_v50: 11.5 ± 0.9 μm; D_v90: 32.3 ± 1.4 μm) and monodisperse. In contrast, in the MSMPR crystallizer, larger crystals were produced with broad and polydisperse CSD (D_v10: 83 ± 19 μm; D_v50: 326 ± 48 μm; D_v90: 577 ± 95 μm). The dissolution profiles of the PFC, MSMPR crystallizer and PF-MSMPR system are presented in Fig. 6.

The PFC product could be featured with fast dissolution as 90 % and 99 % of the ASA was dissolved in 12.5 and 30–40 min, respectively. The larger-sized MSMPR crystallizer product dissolved slower; the 90 % dissolution was reached after ~ 30 min and 99 % after ~ 70 min. The dissolution profile of the sample produced in the PF-MSMPR system was similar to the PFC product; 90 % of the ASA was dissolved in 10–15 min and 99 % in ~ 30 min. Based on the dissolution test results, it is clear

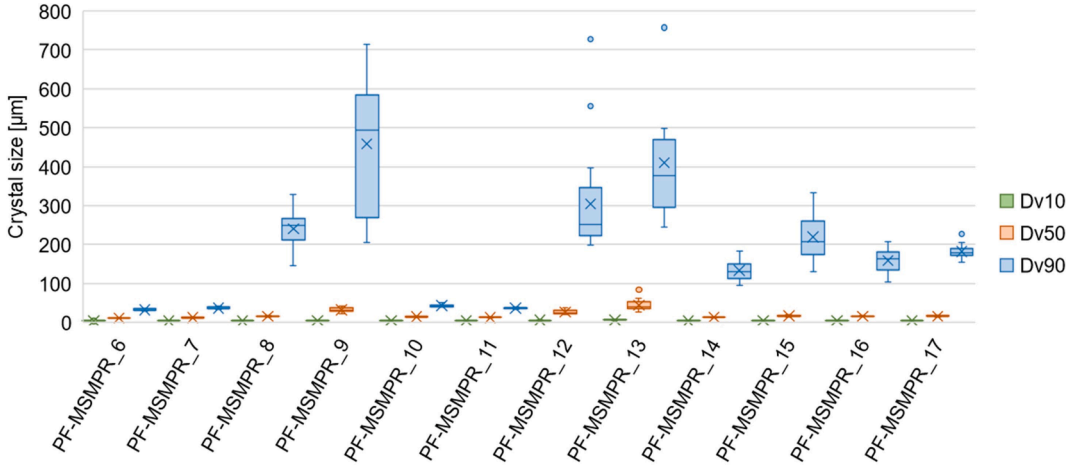

Fig. 4. Average D_v10, D_v50, and D_v90 and their standard deviation in the DoE (PF-MSMPR_6-PF-MSMPR_17).

Table 7
Microscopic Pictures, D_v-values [μm], and CSD Plots of PF-MSMPR_7, _15, and _9 Experiments at 2 °C.

PF-MSMPR_7 T:2°C; K30:1*p*%; TFR:30 mL/min			PF-MSMPR_15 T:2°C; K30:7.5*p*%;TFR:20 mL/min			PF-MSMPR_9 T:2°C; K30:14*p*%; TFR:30 mL/min		
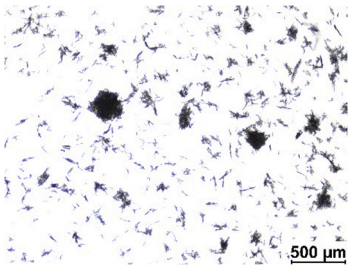			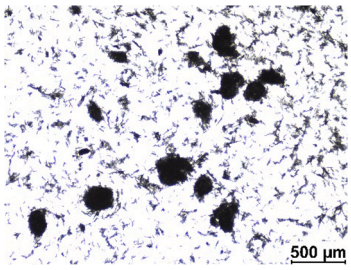			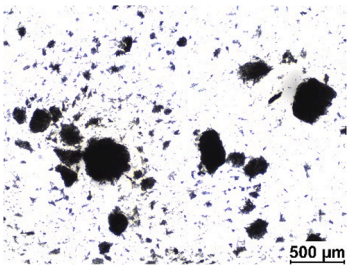		
D_v10	D_v50	D_v90	D_v10	D_v50	D_v90	D_v10	D_v50	D_v90
4.0 ± 0.1	12.4 ± 0.5	37.2 ± 2.6	4.5 ± 0.4	17.1 ± 1.7	219.7 ± 57.4	5.1 ± 0.3	32.7 ± 5.9	458.5 ± 172.1
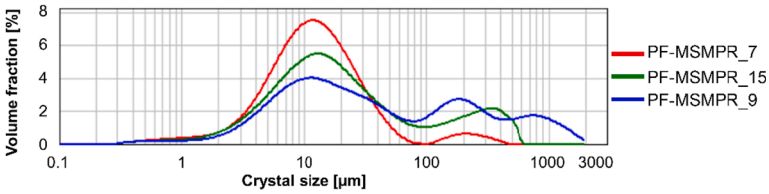								

Table 8
Microscopic Pictures, D_v-values [μm], and CSD Plots of PF-MSMPR_10, _16, and _12 Experiments at 25 °C.

PF-MSMPR_10 T:25 °C; K30:1*p*%; TFR:10 mL/min			PF-MSMPR_16 T:25 °C; K30:7.5*p*%;TFR:20 mL/min			PF-MSMPR_12 T:25 °C; K30:14*p*%; TFR:10 mL/min		
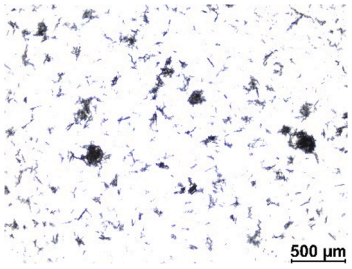			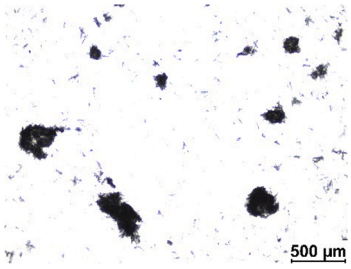			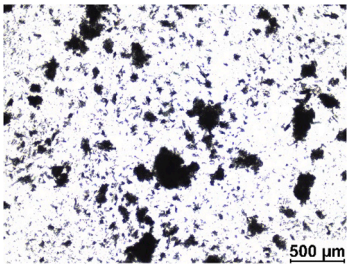		
D_v10	D_v50	D_v90	D_v10	D_v50	D_v90	D_v10	D_v50	D_v90
4.9 ± 0.1	14.7 ± 0.4	43.2 ± 3.6	4.7 ± 0.1	15.9 ± 0.5	158.5 ± 29.6	5.4 ± 0.3	26.3 ± 5.5	304.2 ± 138.1
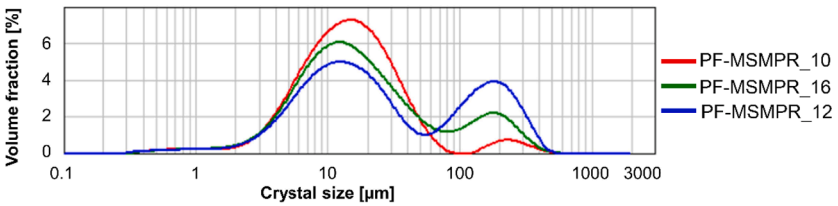								

that PF-MSMPR-produced agglomerates could disintegrate easily in a water solution. The disintegration is induced by the good water solubility of the polymer which acts as a binder between the primary particles. After rapid disintegration of the agglomerate, the crystals behave as individual small crystals similar to those produced in a PFC under similar conditions. In conclusion, the developed crystallizer technology was enabled to modify the particle properties, thus, improving its technological properties by sticking the primary crystals together using a polymer excipient. In the meantime, the favorable dissolution profile of the primary crystals could be preserved.

3.2.5. *Spatially segmented antisolvent dosing*

To illustrate the application possibilities of the developed PF-MSMPR crystallizer system, we performed an additional experiment with spatially segmented antisolvent dosing applying the experience of the previously presented experimental design. According to previous observations, all of the ASA is crystallized in the PFC by ultrasound irradiation; therefore, a quasi-equilibrium state suspension is fed into the MSMPR crystallizer, where only additive-promoted agglomeration of the crystals takes place. To promote nucleation and crystal growth in the MSMPR crystallizer, a supersaturation state must be induced. For this purpose, we applied spatially segmented antisolvent dosing. The flow rate of the antisolvent fed into the PFC was equal to the ASA solution flow rate. Afterward, to reach the desired 4:1 antisolvent to ASA solution ratio, antisolvent was fed into the MSMPR with a 3:1 antisolvent to ASA solution ratio. In this system, PFC functioned as an *in-situ* seed generator. This method enabled to initiate supersaturation in the MSMPR crystallizer section and promoted crystallization in the presence of PVP. Therefore, secondary nucleation and crystal growth could be carried out in MSMPR besides agglomeration of the primary particles. The result of the PF-MSMPR_18 experiment is summarized in Table 9. The segmented antisolvent dosing did not affect the onset of steady-state

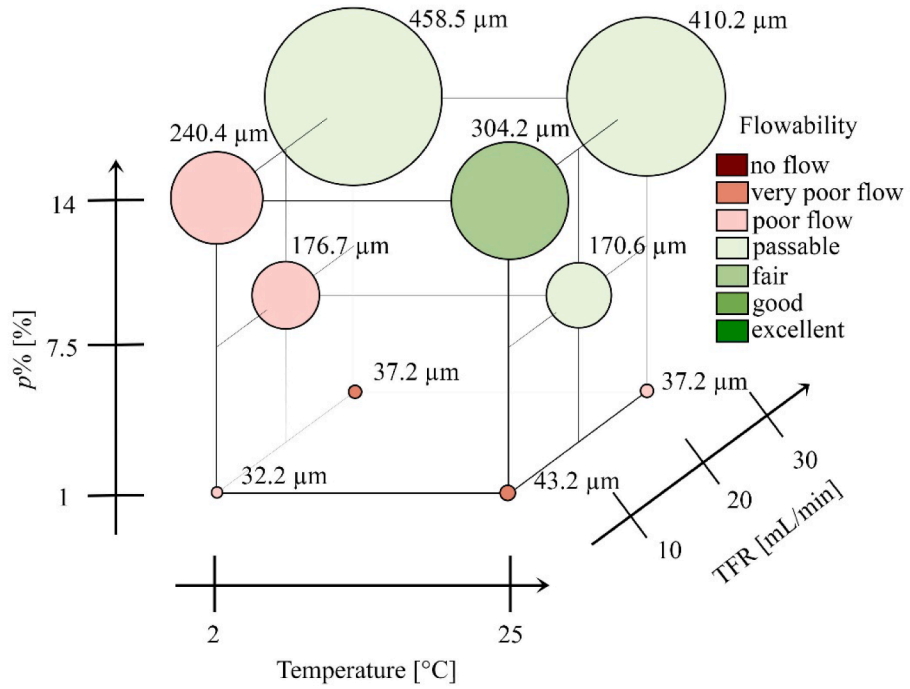

Fig. 5. Classification of the experiments according to the flowability properties and average D_v90-values as a function of process conditions.

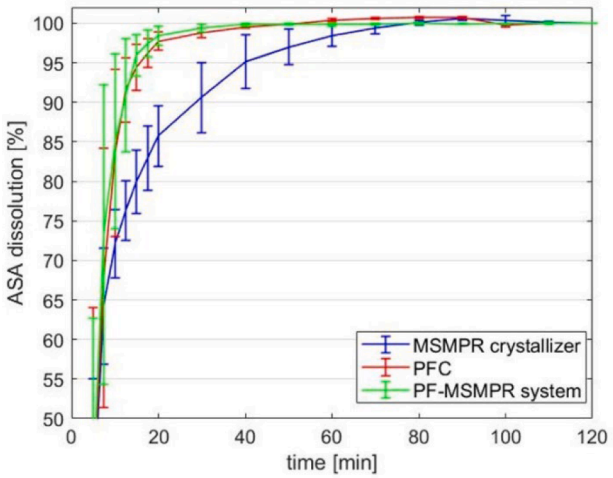

Fig. 6. Dissolution rate of MSMPR_3 (T: 2.5 °C, TFR: 20 mL/min, AS/ASA: 4:1, RT: 11.75 min,), PF_12 (T: 25 °C, AS/ASA: 4:1, RT: 60 *sec*), PF-MSMPR_17 (T: 25 °C, 7.5 *p*%, TFR: 20 mL/min, AS/ASA: 4:1, RT: 12.22 min).

operation; thus, the startup period lasted for 1 RT, similarly to the previous continuous experiments. The product contained 0.47 ± 0.03 % SA, and 8.89 % PVP-K30 was detected with Raman mapping (Fig. 7). The distribution of the polymer on the product surface was slightly more inhomogeneous than in non-segmented dosing experiments. This can be explained by the larger size of the agglomerates (see Table 10.) and thus, the possible size of the remaining mother liquor droplets after heptane washing. Apart from this, the results are similar to the experiments with non-segmented antisolvent dosing.

At the end of the PFC, the yield was 45.5 %. This value increased to 57.4 % on average at the end of the connected crystallizer system. The productivity of the PF-MSMPR system was 12.7 ± 0.3 g/h. The measured yield and productivity are lower than in the previous experiments with similar set conditions (PF-MSMPR_16 and PF-MSMPR_17). This phenomenon could be caused by the segmented antisolvent addition resulting in a modified crystallization mechanism. In this case, in the MSMPR crystallizer, secondary nucleation and crystal growth could occur besides agglomeration. Accordingly, the structure of the resulting

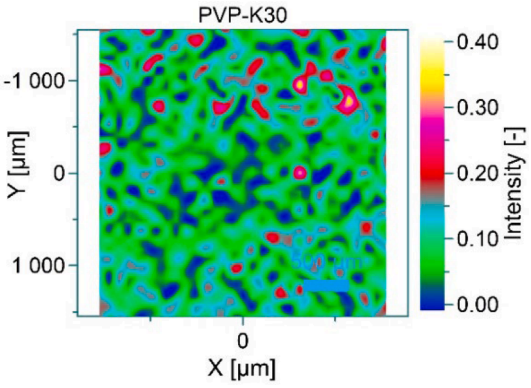

Fig. 7. Distribution of PVP-K30 on the surface of the PF-MSMPR_18 product according to Raman mapping.

Table 9
Result Summary of PF-MSMPR_18 Experiment.

ID of exp.	T [°C]	*p*% [%]	TFR [mL/min]	SA [%]	PVP-K30 [%]	y_{corr} [%] *	Productivity$_{corr}$ [g/h] *	Flowability
PF-MSMPR_18	25	7.5	20	0.47 ± 0.03	8.89	57.4 ± 1.3	12.7 ± 0.3	good

* Pure ASA yield and productivity corrected with the amount of PVP in the product.

Table 10
Microscopic Pictures, D_v-values [μm], and CSD Plots of PF-MSMPR_18 (PFC), PF-MSMPR_18 (final), and PF-MSMPR_16 Experiment Product.

PF-MSMPR_18 (PFC product)			PF-MSMPR_18			PF-MSMPR_16		
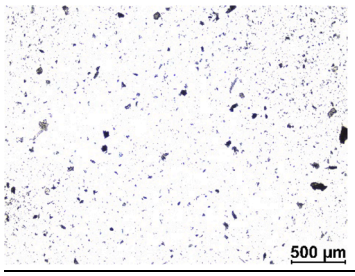			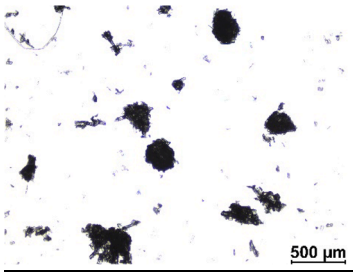			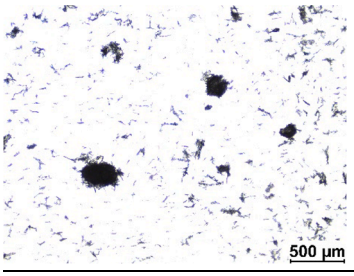		
D_v10	D_v50	D_v90	D_v10	D_v50	D_v90	D_v10	D_v50	D_v90
4.4 ± 0.2	13.2 ± 0.6	36.2 ± 8.6	11.5 ± 1.2	76.9 ± 22.7	352.1 ± 71.2	4.7 ± 0.1	15.9 ± 0.5	158.5 ± 29.6

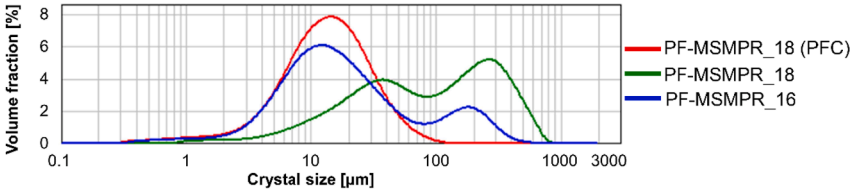

agglomerates is different compared to the non-segmented antisolvent addition method.

We illustrated the crystal habit of the product collected at the end of the PFC (PF-MSMPR_18, PFC product) and MSMPR (PF-MSMPR_18) during the spatially segmented antisolvent dosing experiment, with the microscopic pictures, D_v-values, and CSD in Table 10. The PF-MSMPR_16 experiment product was also presented to compare the crystal habit of segmented and non-segmented antisolvent dosing.

The PF-MSMPR_18 PFC product contained small, 10–20 μm columnar crystals. The CSD measurement resulted in unimodal CSD (Table 10). The particle size of the PF-MSMPR_18 PFC product (red curve) is similar to the first crystal fraction of the previously discussed bimodal PF-MSMPR_16 product (blue curve). However, it is worth studying the microscopic images to interpret the CSD curve of the PF-MSMPR_18 product.

In the microscopic pictures of the PF-MSMPR_18 product, larger primary particles could be observed in the agglomerates since the small particles produced in the PFC could grow in the MSMPR crystallizer. Besides, here the polymer-induced agglomeration is also significant. The small crystals could stick together or stick to the surface of larger particles resulting in different sizes of agglomerates. Due to the agglomeration process, the PF-MSMPR_18 final product CSD was bimodal similar to the PF-MSMPR_16 product, but the smaller-sized crystal fraction peak ranged in 30–40 μm is bigger than in the case of PF-MSMPR_16 (peak sized in 10–20 μm). The larger-sizes crystal fraction size was also bigger (200–400 μm). The ratio of crystal fractions was different since the larger-sized crystal fraction volume was higher. In conclusion, it can be assumed that the crystal growth and agglomeration were the dominant subprocesses in the MSMPR crystallizer, as the size of both crystal fractions was increased and no peak indicating intensive secondary nucleation was found in the CSD curve.

The product was classified as "good" regarding flowability, as the Hausner ratio and Carr index were 1.14 ± 0.01 and 12.5 ± 0.7, respectively. The 90 % of ASA was dissolved in 15 min and 99 % in 40–50 min; thus, the dissolution rate of the product was slightly slower compared to the product collected from the PF-MSMPR system operated with non-segmented antisolvent addition. The slightly slower dissolution could be explained by the larger primary particles that built up the agglomerates in the PF-MSMPR_18 product. However, this dissolution was significantly faster than the dissolution of a separate MSMPR crystallizer product, presumably due to the fast disintegration of agglomerates (Fig. 8).

The procedure presented in this section may be a promising particle properties modification strategy. The results show that the supersaturation increased the size of the individual crystals in the MSMPR crystallizer while the added excipient promoted agglomeration. The investigated method can shorten the long setup period of MSMPR crystallizers while producing a product with good technological properties and a favorable dissolution profile with high yield and purity.

4. Conclusions

We developed a robust connected crystallization technology comprising PFC and MSMPR crystallizer to process a multicomponent ASA reaction mixture with a polymer additive. It was possible to combined the advantages of the two continuous crystallisation technologies to produce a crystalline product with fast dissolution but easy processability. We aimed to improve the processability of the small-sized crystals produced in PFC via agglomeration with the aid of excipient fed into the MSMPR crystallizer, thereby making certain formulation

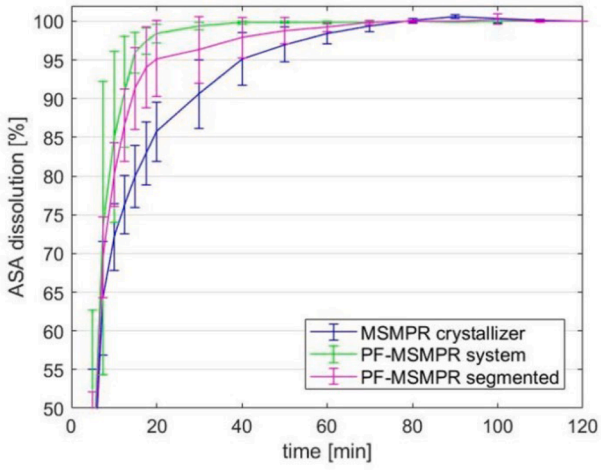

Fig. 8. Dissolution rate of an MSMPR product (T: 2.5 °C, TFR: 20 mL/min, RT: 11.75 min), a PF-MSMPR system operated with non-segmented antisolvent dosing (T: 25 °C, 7.5 *p*%, TFR: 20 mL/min, RT: 12.22 min), and a PF-MSMPR system operated with segmented antisolvent addition (T: 25 °C, 7.5 *p*%, TFR: 20 mL/min, RT: 12.98 min).

steps (e.g., granulation) unnecessary.

The experimental results showed that crystallization additive is essential for the agglomerate formation, and merely the connection of the crystallizers could not promote particle properties modification. After testing various additives, we applied PVP-K30/water solution to facilitate the agglomeration of primary particles in continuous experiments.

The developed technology was operated with a short onset period, effectively reducing the inconsistent waste product amount produced until reaching the steady-state operation. By investigating the crystallization process parameter effect on product composition, we found that the SA impurity content could be reduced to 0.39 ± 0.21 % regardless of the crystallization conditions. The PVP-K30 additive content of the product was increased by applying a higher amount of polymer. However, above 7 *p*% used, the product polymer content could not rise significantly. The corrected yield of the developed technology could be described with a linear model as a function of temperature, and it ranged between 63 and 85 %, while the productivity was 7.3–28.1 g/h. The product of the PF-MSMPR system was polydisperse, indicating the formation of agglomerates. The scale of agglomeration initially depended on the amount of polymer used. By small *p*%, the product particle properties were not significantly different from the simple PFC product. In the case of higher *p*% (7.5–14 %), besides small columnar primary particles (10–20 μm), larger agglomerates (100–500 μm) appeared, improving the technological properties of the product. The best flowability achieved was "fair" (T: 25 °C; K30: 14 *p*%; TFR: 10 mL/min), while the dissolution rate was similarly favorable to the primary PFC-produced crystals (90 % dissolved in 10–15 min).

With spatially segmented antisolvent addition, the system could be operated with similar product composition but lower yield and productivity. This technology enhanced the crystal growth and also agglomeration, increasing the size of each particle fraction. As a result, the product flowability was classified as "good"; however, the dissolution rate was as fast as that of the PFC product.

The developed additive-assisted continuous crystallization in a connected crystallizer system offers the production of crystalline material with good flowability (i.e., processability) and fast dissolution properties. While further, unexplored possibility lies in spatially segmented antisolvent dosing.

CRediT authorship contribution statement

Kornélia Tacsi: Conceptualization, Methodology, Investigation, Validation, Visualization, Writing – original draft, Writing – review & editing. **György Stoffán:** Investigation. **Dorián László Galata:** Formal analysis. **Éva Pusztai:** Formal analysis. **Martin Gyürkés:** Formal analysis. **Brigitta Nagy:** Conceptualization. **Botond Szilágyi:** Conceptualization. **Zsombor Kristóf Nagy:** Conceptualization. **György Marosi:** Conceptualization, Supervision, Writing – review & editing. **Hajnalka Pataki:** Conceptualization, Methodology, Supervision, Writing – review & editing.

Declaration of Competing Interest

The authors declare that they have no known competing financial interests or personal relationships that could have appeared to influence the work reported in this paper.

Data availability

Data will be made available on request.

Acknowledgement

This work was financially supported by the National Research Development and Innovation Office of Hungary (K-143039, FK-132133, FK-143019, PD-142970, FK-138475). Hajnalka Pataki and Brigitta Nagy is thankful for the János Bolyai Research Scholarship of the Hungarian Academy of Sciences. The research was funded by the National Research, Development and Innovation Fund of Hungary in the frame of the 2019–1.3.1-KK-2019–00004 project. The research was also supported by the ÚNKP-22-3-II-BME-171, ÚNKP-22-4-II-BME-137 and ÚNKP-22-5-BME-300 New National Excellence Program of the Ministry for Culture and Innovation from the source of the National Research, Development and Innovation Fund. The authors thank Egis Pharmaceuticals PLC for supporting the research with the overflow crystallizer device.

Appendix A. Supplementary material

Supplementary data to this article can be found online at https://doi.org/10.1016/j.ijpharm.2023.122725.

References

Acevedo, D., Yang, X., Liu, Y.C., O'Connor, T.F., Koswara, A., Nagy, Z.K., Madurawe, R., Cruz, C.N., 2019. Encrustation in Continuous Pharmaceutical Crystallization Processes - A Review. Org. Process Res. Dev. 23, 1134–1142. https://doi.org/10.1021/acs.oprd.9b00072.

Agnew, L.R., McGlone, T., Wheatcroft, H.P., Robertson, A., Parsons, A.R., Wilson, C.C., 2017. Continuous Crystallization of Paracetamol (Acetaminophen) Form II: Selective Access to a Metastable Solid Form. Cryst. Growth Des. 17, 2418–2427. https://doi.org/10.1021/acs.cgd.6b01831.

Arribas Bueno, R., Crowley, C.M., Davern, P., Hodnett, B.K., Hudson, S., 2018. Heterogeneous Crystallization of Fenofibrate onto Pharmaceutical Excipients. Cryst. Growth Des. 18, 2151–2164. https://doi.org/10.1021/acs.cgd.7b01598.

Balogh, A., Domokos, A., Farkas, B., Farkas, A., Rapi, Z., Kiss, D., Nyiri, Z., Eke, Z., Szarka, G., Örkényi, R., Mátravölgyi, B., Faigl, F., Marosi, G., Nagy, Z.K., 2018. Continuous end-to-end production of solid drug dosage forms: Coupling flow synthesis and formulation by electrospinning. Chem. Eng. J. 350, 290–299. https://doi.org/10.1016/j.cej.2018.05.188.

Borsos, A., Majumder, A., Nagy, Z.K., 2016. Multi-Impurity Adsorption Model for Modeling Crystal Purity and Shape Evolution during Crystallization Processes in Impure Media. Cryst. Growth Des. 16, 555–568. https://doi.org/10.1021/acs.cgd.5b00320.

Chadwick, K., Chen, J., Myerson, A.S., Trout, B.L., 2012. Toward the rational design of crystalline surfaces for heteroepitaxy: Role of molecular functionality. Cryst. Growth Des. 12, 1159–1166. https://doi.org/10.1021/cg2010858.

Erdemir, D., Rosenbaum, T., Chang, S.Y., Wong, B., Kientzler, D., Wang, S., Desai, D., Kiang, S., 2018. Novel Co-processing Methodology to Enable Direct Compression of a Poorly Compressible, Highly Water-Soluble Active Pharmaceutical Ingredient for Controlled Release. Org. Process Res. Dev. 22, 1383–1392. https://doi.org/10.1021/acs.oprd.8b00204.

Erdemir, D., Daftary, V., Lindrud, M., Buckley, D., Lane, G., Malsbury, A., Tao, J., Kopp, N., Hsieh, D.S., Nikitczuk, W., Engstrom, J.D., 2019. Design and Scale-up of a Co-processing Technology to Improve Powder Properties of Drug Substances. Org. Process Res. Dev. 23, 2685–2698. https://doi.org/10.1021/acs.oprd.9b00354.

Furuta, M., Mukai, K., Cork, D., Mae, K., 2016. Continuous crystallization using a sonicated tubular system for controlling particle size in an API manufacturing process. Chem. Eng. Process. Process Intensif. 102, 210–218. https://doi.org/10.1016/j.cep.2016.02.002.

Gao, Z., Wu, Y., Gong, J., Wang, J., Rohani, S., 2018. Continuous crystallization of α-form L-glutamic acid in an MSMPR-Tubular crystallizer system. J. Cryst. Growth. https://doi.org/10.1016/j.jcrysgro.2018.07.007.

Hu, C., Testa, C.J., Shores, B.T., Wu, W., Shvedova, K., Born, S.C., Chattopadhyay, S., Takizawa, B., Mascia, S., 2019. An experimental study on polymorph control and continuous heterogeneous crystallization of carbamazepine. CrstEngComm 21, 5076–5083. https://doi.org/10.1039/c9ce00908f.

Hu, C., Shores, B.T., Derech, R.A., Testa, C.J., Hermant, P., Wu, W., Shvedova, K., Ramnath, A., Al Ismaili, L.Q., Su, Q., Sayin, R., Born, S.C., Takizawa, B., O'Connor, T.F., Yang, X., Ramanujam, S., Mascia, S., 2020. Continuous reactive crystallization of an API in PFR-CSTR cascade with in-line PATs. React. Chem. Eng. 5, 1950–1962. https://doi.org/10.1039/d0re00216j.

Kaialy, W., Maniruzzaman, M., Shojaee, S., Nokhodchi, A., 2014. Antisolvent precipitation of novel xylitol-additive crystals to engineer tablets with improved pharmaceutical performance. Int. J. Pharm. 477, 282–293. https://doi.org/10.1016/j.ijpharm.2014.10.015.

Koyama, M., Kudo, S., Amari, S., Takiyama, H., 2020. Development of novel cascade type crystallizer for continuous production of crystalline particles. J. Ind. Eng. Chem. 89, 111–114. https://doi.org/10.1016/j.jiec.2020.06.021.

Kutluay, S., Abdullah Ceyhan, A., Sahin, Ö., Sait Izgi, M., 2020. Utilization of in situ FBRM and PVM probes to analyze the influences of monopropylene glycol and oleic acid as novel additives on the properties of boric acid crystals. Ind. Eng. Chem. Res. 59, 9198–9206. https://doi.org/10.1021/acs.iecr.0c00551.

Li, X., Xu, D., Yang, J., Yan, Z., Luo, T., Li, X., Zhang, Z., Wang, X., 2021. Utilization of FBRM and PVM to analyze the effects of different additives on the crystallization of

ammonium dihydrogen phosphate. J. Cryst. Growth. 576, 126378 https://doi.org/10.1016/j.jcrysgro.2021.126378.
Liu, W.J., Ma, C.Y., Wang, X.Z., 2015. Novel impinging jet and continuous crystallizer design for rapid reactive crystallization of pharmaceuticals. Procedia Eng. 102, 499–507. https://doi.org/10.1016/j.proeng.2015.01.199.
Liu, W.J., Ma, C.Y., Liu, J.J., Zhang, Y., Wang, X.Z., 2017. Continuous Reactive Crystallization of Pharmaceuticals Using Impinging Jet Mixers. Process Syst. Engin. 63, 967–974. https://doi.org/10.1002/aic.15438.
Mathew Thomas, K., Nyande, B.W., Lakerveld, R., 2022. Design and characterization of Kenics static mixer crystallizers. Chem. Eng. Res. Des. 179, 549–563. https://doi.org/10.1016/j.cherd.2022.01.025.
Mou, M., Jiang, M., 2020. Fast Continuous Non-Seeded Cooling Crystallization of Glycine in Slug Flow: Pure α-Form Crystals with Narrow Size Distribution. J. Pharm. Innov. 15, 281–294. https://doi.org/10.1007/s12247-020-09438-0.
Nagy, Z.K., El Hagrasy, A., Litster, J., 2020. Continuous Pharmaceut. Process.
Nagy, Z.K., Szilagyi, B., Pal, K., Tabar, I.B., 2020. A novel robust digital design of a network of industrial continuous cooling crystallizers of dextrose monohydrate: From laboratory experiments to industrial application. Ind. Eng. Chem. Res. 59, 22231–22246. https://doi.org/10.1021/acs.iecr.0c04870.
Nagy, B., Szilágyi, B., Domokos, A., Vészi, B., Tacsi, K., Rapi, Z., Pataki, H., Marosi, G., Nagy, Z.K., Nagy, Z.K., 2021. Dynamic flowsheet model development and digital design of continuous pharmaceutical manufacturing with dissolution modeling of the final product. Chem. Eng. J., 129947 https://doi.org/10.1016/j.cej.2021.129947.
Nokhodchi, A., Amire, O., Jelvehgari, M., 2010. Physico-mechanical and dissolution behaviours of ibuprofen crystals crystallized in the presence of various additives. Daru 18, 74–83.
Pfund, L.Y., Price, C.P., Frick, J.J., Matzger, A.J., 2015. Controlling pharmaceutical crystallization with designed polymeric heteronuclei. J. Am. Chem. Soc. 137, 871–875. https://doi.org/10.1021/ja511106j.
Powell, K.A., Saleemi, A.N., Rielly, C.D., Nagy, Z.K., 2016. Monitoring Continuous Crystallization of Paracetamol in the Presence of an Additive Using an Integrated PAT Array and Multivariate Methods. Org. Process Res. Dev. 20, 626–636. https://doi.org/10.1021/acs.oprd.5b00373.
Quon, J.L., Chadwick, K., Wood, G.P.F., Sheu, I., Brettmann, B.K., Myerson, A.S., Trout, B.L., 2013. Templated nucleation of acetaminophen on spherical excipient agglomerates. Langmuir 29, 3292–3300. https://doi.org/10.1021/la3041083.
Rosenbaum, T., Erdemir, D., Chang, S.Y., Kientzler, D., Wang, S., Chan, S.H., Brown, J., Hanley, S., Kiang, S., 2018. A novel co-processing method to manufacture an API for extended release formulation via formation of agglomerates of active ingredient and hydroxypropyl methylcellulose during crystallization. Drug Dev. Ind. Pharm. 44, 1606–1612. https://doi.org/10.1080/03639045.2018.1483386.
Sangwal, K., 2007. Additives and crystallization processes. https://doi.org/10.1016/b978-0-12-558820-1.50007-7.
Schenck, L., Erdemir, D., Saunders Gorka, L., Merritt, J.M., Marziano, I., Ho, R., Lee, M., Bullard, J., Boukerche, M., Ferguson, S., Florence, A.J., Khan, S.A., Sun, C.C., 2020. Recent Advances in Co-processed APIs and Proposals for Enabling Commercialization of These Transformative Technologies. Mol. Pharm. 17, 2232–2244. https://doi.org/10.1021/acs.molpharmaceut.0c00198.
Simone, E., Cenzato, M.V., Nagy, Z.K., 2016. A study on the effect of the polymeric additive HPMC on morphology and polymorphism of ortho-aminobenzoic acid crystals. J. Cryst. Growth. 446, 50–59. https://doi.org/10.1016/j.jcrysgro.2016.04.034.
Sonnenschein, J., Wohlgemuth, K., 2022. Archimedes tube crystallizer: Design and characterization for small-scale continuous crystallization. Chem. Eng. Res. Des. 178, 488–501. https://doi.org/10.1016/j.cherd.2021.12.017.
Tacsi, K., Pataki, H., Domokos, A., Nagy, B., Csontos, I., Markovits, I., Farkas, F., Nagy, Z. K., Marosi, G., 2020. Direct Processing of a Flow Reaction Mixture Using Continuous Mixed Suspension Mixed Product Removal Crystallizer. Cryst. Growth Des. 20, 4433–4442. https://doi.org/10.1021/acs.cgd.0c00252.
Tacsi, K., Joo, A., Pusztai, E., Domokos, A., Nagy, Z.K., Marosi, G., Pataki, H., 2021. Development of a Triple Impinging Jet Mixer for Continuous Antisolvent Crystallization of Acetylsalicylic Acid Reaction Mixture. Chem. Eng. Process. - Process Intensif., 108446 https://doi.org/10.1016/j.cep.2021.108446.
Tacsi, K., Stoffán, G., Pusztai, É., Nagy, B., Domokos, A., Szilágyi, B., Nagy, Z.K., Marosi, G., Pataki, H., 2022. Implementation of sonicated continuous plug flow crystallization technology for processing of acetylsalicylic acid reaction mixture. Powder Technol. 400, 117255 https://doi.org/10.1016/j.powtec.2022.117255.
Testa, C.J., Shvedova, K., Hu, C., Wu, W., Born, S.C., Takizawa, B., Mascia, S., 2021. Heterogeneous Crystallization as a Process Intensification Technology in an Integrated Continuous Manufacturing Process for Pharmaceuticals. Org. Process Res. Dev. 25, 225–238. https://doi.org/10.1021/acs.oprd.0c00468.
van der Leeden, M.C., Kashchiev, D., van Rosmalen, G.M., 1993. Effect of additives on nucleation rate, crystal growth rate and induction time in precipitation. J. Cryst. Growth. 130, 221–232. https://doi.org/10.1016/0022-0248(93)90855-Q.
Verma, V., Peddapatla, R.V.G., Crowley, C.M., Crean, A.M., Davern, P., Hudson, S., Hodnett, B.K., 2018. Experimental Study on the Influence of Excipients on the Heterogeneous Crystallization and Dissolution Properties of an Active Pharmaceutical Ingredient. Cryst. Growth Des. 18, 338–350. https://doi.org/10.1021/acs.cgd.7b01336.
Wang, L., Tang, W., Du, S., Wu, S., Gong, J., 2020. Additive-Induced Selective Crystallization of the Elusive Form-II of γ-Aminobutyric Acid. Chem. Eng. Technol. 43, 1137–1143. https://doi.org/10.1002/ceat.201900639.
Wu, W.L., Oliva, J.A., Kshirsagar, S., Burcham, C.L., Nagy, Z.K., 2021. Continuous in Situ Seed Generation through the Integration of a Mixed Suspension Mixed Product Removal and an Oscillatory Baffled Crystallizer for the Control of Crystal Size Distribution and Polymorphic Form. Cryst. Growth Des. 21, 6684–6696. https://doi.org/10.1021/acs.cgd.1c00301.
Yang, Y., Nagy, Z.K., 2015. Combined cooling and antisolvent crystallization in continuous mixed suspension, mixed product removal cascade crystallizers: Steady-state and startup optimization. Ind. Eng. Chem. Res. 54, 5673–5682. https://doi.org/10.1021/ie5034254.
Yazdanpanah, N., Testa, C.J., Perala, S.R.K., Jensen, K.D., Braatz, R.D., Myerson, A.S., Trout, B.L., 2017. Continuous Heterogeneous Crystallization on Excipient Surfaces. Cryst. Growth Des. 17, 3321–3330. https://doi.org/10.1021/acs.cgd.7b00297.
Yilmaz, Y., Atassi, F., Sanchez-Felix, M., 2017. The application of crystallization in the presence of additives to enable drug-in-capsule technology. Pharm. Dev. Technol. 22, 804–808. https://doi.org/10.1080/10837450.2016.1190748.
Zhang, D., Xu, S., Du, S., Wang, J., Gong, J., 2017. Progress of pharmaceutical continuous crystallization. Engineering 3, 354–364. https://doi.org/10.1016/J.ENG.2017.03.023.